PROCEEDINGS, 48th Workshop on Geothermal Reservoir Engineering
Stanford University, Stanford, California, February 6-8, 2023
SGP-TR-224

Laboratory Evaluation of the Short-Term Clogging Behavior of Various Materials and Their Combined Use for Lost Circulation Management

Seiji Nakagawa[1], Chun Chang[1], William Kibikas[2], Timothy Kneafsey[1], Patrick Dobson[1], Abraham Samuel[3] and Stephen J. Bauer[2]

[1]Lawrence Berkeley National Laboratory, Berkeley, CA 94720, [2]Sandia National Laboratories, Albuquerque, NM 87185, [3]Geothermal Resource Group Inc., Palm Desert, California, USA

snakagawa@lbl.gov[1], chunchang@lbl.gov[1], wmkibiks@sandia.gov[2], tkneafsey@lbl.gov[1], pfdobson@lbl.gov[1], samabraham@geothermalresourcegroup.com[3], sjbauer001@gmail.com[2]

Keywords: lost circulation materials; fracture; clogging; laboratory experiment

ABSTRACT

Laboratory experiments were conducted to examine the clogging behavior of several commonly deployed commercial fluid-loss control materials (Lost circulation materials) in single fractures and fracture zones, testing both single materials and combinations. A commercial high-temperature, high-pressure permeability plugging tester (Ofite, TX) was modified for improved flow, pressure, and temperature control. Additionally, a new internal test module for this tester containing a model glass fracture or a pack of glass beads was developed to examine the performance of the materials, rather than using standard porous plates and slotted disks. Using this test system, a series of clogging tests was conducted at 90 ˚C. Lost circulation materials were added to a synthetic drilling fluid containing bentonite clay, which was flowed through the fracture model by rapidly increasing the differential pressure across the test module (7.62 cm long) up to 3.4 MPa. The results generally showed superior performance gained from combinations of lost circulation materials compared to single material tests. To better understand the mechanism of plug formation and permeability reduction, we also used a simple one-dimensional consolidation model to predict the evolution of the overall plug compaction and flow reduction. The key inputs required by this model are the nonlinear stress-strain relationship and the stress-dependent permeability of the plug materials, which may be determined via laboratory experiments involving a small flow-through compaction cell. The modeling results indicate that rapid reduction of permeability compared to the compaction of a lost circulation material can lead to abrupt, highly efficient clogging of a fracture, which may help explain observed very small fluid loss for some of the materials used in the experiments.

1. INTRODUCTION

Excessive fluid loss during drilling causes a variety of problems, including increased friction, the arrest of a drill string, loss of information from returning mud and drill cuttings, underbalanced mud pressure and formation fluid influx, and the potential loss of the drill string and the borehole. Fluid loss causes substantial disruption to drilling operations and increases the risk and the cost of drilling during a geothermal project. In the field, a variety of both natural and synthetic materials have been used to reduce or stop fluid loss by inducing clogging of high-permeability fractures and fracture zones. Both granular and fibrous materials are used in conjunction with drilling fluid viscosity modification. For effective clogging, the lost circulation materials first need to take a foothold within and/or at the entrance to a fracture, then stop fluid flow by reducing the permeability of the accumulated material (filtration cake).

Lost circulation materials (LCMs) that are generally available include granular and fibrous materials or mixes and may be mineral or organic in nature. These include Magma fiber, calcium carbonate chips, graphite, diatomaceous earth, bentonite, cottonseed hulls, various sizes of nut shells, sawdust, commercial blends of materials, and other available inexpensive materials that are conducive to clogging. For use in geothermal drilling, consideration must be given to whether the lost circulation (LC) event occurred above the reservoir, which is cooler and the applied LCM will not damage the reservoir, or in the hotter reservoir (Winn et al., 2023). Above the reservoir, standard oil and gas LCMs and protocols may be used. Within the reservoir, however, LC may indicate a feed zone. Although near-wellbore conditions in the reservoir may be significantly cooler than the ambient reservoir temperature, treatment of LC in the hot reservoir requires consideration of the potential consequences of not treating the lost circulation, treating the LC with materials that may not be removable (e.g., bentonite, graphite), treating the LC with materials that thermally degrade (e.g., organic materials, Kibikas et al., 2023), and treating the LC with materials that are chemically removable (e.g., calcium carbonate can be removed with acid). Most LCMs have not been well-studied under geothermal conditions.

Laboratory-observed behavior of permeability-controlling materials (lost-circulation materials, or, LCMs) can be generally categorized into four types: (1) no clogging (flow through); (2) blocking but with flow through; (3) clogging (permeability blocking); and (4) dynamic partial blocking with pressure/flow oscillations (Figure 1). LCMs with small grain sizes compared to the fracture aperture can simply flow into the fracture and get lost. In contrast, large-grain-size LCMs block the fracture entrance by “bridging”, but the drilling fluid can still flow through the pores. LCMs with a proper grain size distribution would produce a filtration cake that can both “bridge” a fracture and stop the fluid flow. For optimal performance of LCMs, for granular materials, several “rules” are available in the literature prescribing the grain size distribution. These rules include the Abram’s Rule (D50 > 1/3 the average pore size), the D90 Rule (D90 = the average pore size), the Vicker’s Method (D90 = the largest pore throat, D75 < 2/3 of the largest pore throat, D50 > 1/3 of the average pore throat, D25 = 1/7 of the mean pore throat, and D10 > the smallest pore size), the Halliburton Method (D50 = the fracture width), and the Alsaba Method (D50 > 0.3 of the fracture width, and D90 > 1.2 times the fracture width) (e.g., Alsaba et al., 2017; Vivas and Salehi, 2022).

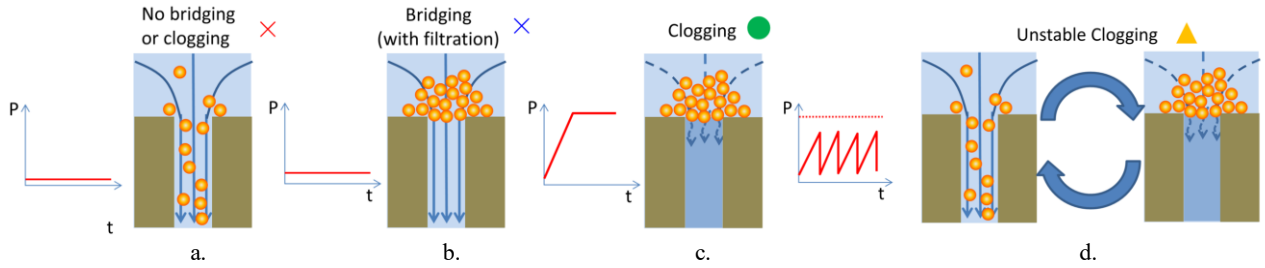

Figure 1: Categorization of typically observed LCM interaction with a fracture in the laboratory. When the pressure in the borehole (P) is increased, the induced flow may result in simple loss of small LCM particles (a), or a permeable filtration cake ("bridge") (b), or successful clogging which stops the fluid loss (c). Insufficient strength of the filter cake can lead to cycling formation of a filter cake and its collapse (d).

In spite of these rules, the dimensions and distributions of the pores and fractures sizes intersected are rarely known, nor is it desirable to stop drilling long enough to quantify these sizes, obtain and mix the suggested particle size distribution. Repeated drilling in a field where controlling LC events has been successful often can inform subsequent drilling, allowing having likely successful materials on hand. Often the approach, however, is to apply what is perceived to be the least expensive and available LCM in an attempt to heal the LC event, and if unsuccessful continue with what is perceived to be more expensive materials until the LC event is healed, it is decided to drill blind, or cement plug is attempted. Cement plugs are not always successful as the cement can be lost to the formation like the drilling fluid (Winn et al., 2023). Lowry et al. (2022) point out that often the most economical approach is the one that heals the LC event with any material as soon as possible, because the cost of delaying this may greatly exceed the cost of the LCM itself.

It is also important to note that clogging and permeability reduction of fractures by LCMs can be dynamic (Figure 1d). With increasing differential pressure across a filter cake, insufficient strength in the cake leads to its cycling formation and collapse. Further, if the structural integrity of the filter cake can hold, the flow-induced, elevated effective stress can increase shear strength by compaction and decrease the permeability. Such behavior implies that the mechanical properties, and the accompanying changes in the permeability, are also important for understanding and optimizing the performance of LCMs, in addition to their grain sizes.

In the following sections of the paper, we present a series of laboratory fracture clogging experiments conducted using several commercially available, commonly used LCMs. The objective of the study is to evaluate the performance of different types of LCMs and their combinations for stopping fluid loss from a fracture during rapid pressurization. We also present preliminary results of numerical modeling of filtration cake permeability evolution, which is conducted to gain better understanding of the role of filtration cake deformation in reducing the fracture permeability.

2. FRACTURE CLOGGING EXPERIMENTS

We conducted clogging and permeability reduction experiments on single fractures by using a commercial, temperature-controlled permeability plugging tester with slots in stainless steel disks representing fracture entry points, and in fracture analogs that were custom manufactured for use in our plugging tester. All the experiments were conducted at 90°C. The primary objective of this test was to examine the impact of LCM types used for permeability reduction, finite fracture depth (in the flow direction), and fracture roughness, on the overall fracture clogging behavior in a short duration (<30 minutes).

2.1 Experimental Setup

2.1.1 Materials

Five different types of LCM were used in the experiment (Figure 2a), these are micronized cellulosic (micro-C, μ-C) particles (both coarse granules and fine powder), cotton seed hulls, cedar fibers, saw dust, which were provided by Sinclair Well Products, and a special blend of various types of LCMs (WCA300), which was used with a high-temperature-resisting specialized polysaccharide gellant (WCA100), provided by North Star Energy Products. The particle size distributions via sieve analysis are shown in Figure 2b, including the result for the fine micro-C powder obtained from a dynamic light scattering (DLS) technique. Additionally, selected types of LCMs were blended (50:50 by weight) to achieve a wider particle size distribution and clogging characteristics.

The fluid transporting LCM particles within a high-temperature geothermal reservoir usually has a low viscosity. Because our experimental setup did not allow us to suspend the particles dynamically as is done in the field, a bentonite (MX-80) mud was used, except for the WCA-type LCM, which is used with its own special fluid thickening agent. A solid-to-fluid weight ratio of 1:10 was used for the mud. This ratio is rather high for typically used drilling fluid, but was necessary to keep the LCMs suspended in the fluid. The viscosity of the mud at ambient conditions using a Marsh cone viscometer was 34–36 cP. (Note that the use of bentonite mud in an actual reservoir while drilling in the expected production zone is not recommended because of the potential formation damage from baked mud.)

Except for the WCA-type LCM, all other types of LCMs (including 50:50 blends) were introduced in the fluid by a solid weight ratio of 5 wt%, and "cured" over 18 hours under the room temperature before the test, for potential time-dependent dispersal of the clay and fine LCM particles and absorption of water. Note that the time between mixing and injection into a well in the field is normally much shorter than this.

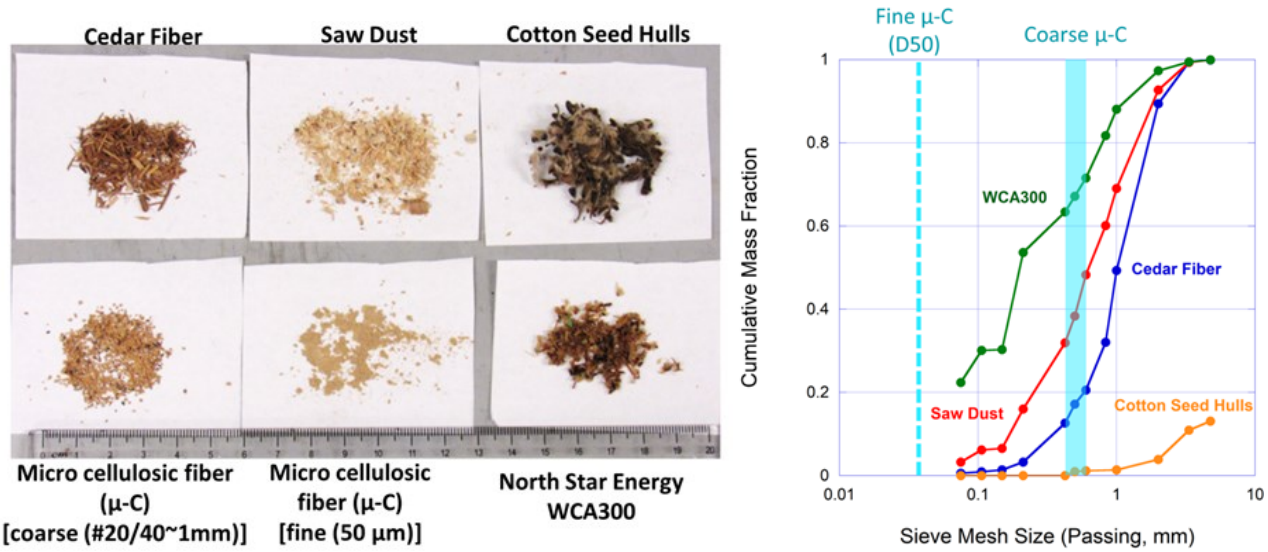

a. Photographs of the tested materials b. Particle size distributions

Figure 2: Lost-circulation materials used in our experiment. These samples obtained from commercial sources (a) were tested as received without additional particle size control. Note that the particle size distribution for cedar fiber samples are very narrow because it corresponds primarily to the thickness of individual needles (b). Also, a large portion of the cotton seed hulls did not pass through the largest 10 mm sieve, because the included cotton fibers had a tendency to clump the hulls together.

2.1.2 Equipment

We used a commercial permeability plugging tester (6,000 psi model, Ofite, TX) for the tests with some modifications (Figure 3a). First, for improved temperature control and safety, an independent temperature controller (Oakton 9500) was added to the power supply. In addition, for controlling the fluid pressure and the flow rate, a syringe pump (ISCO/Teledyne 500D) was used to inject the drive fluid (water) into the lower chamber of the tester. Lastly, in order to test clogging of a fracture that is more realistic than commonly used slotted discs for this type of experiment, we developed an internal module that can house fracture(s) with a range of geometries (Figure 4).

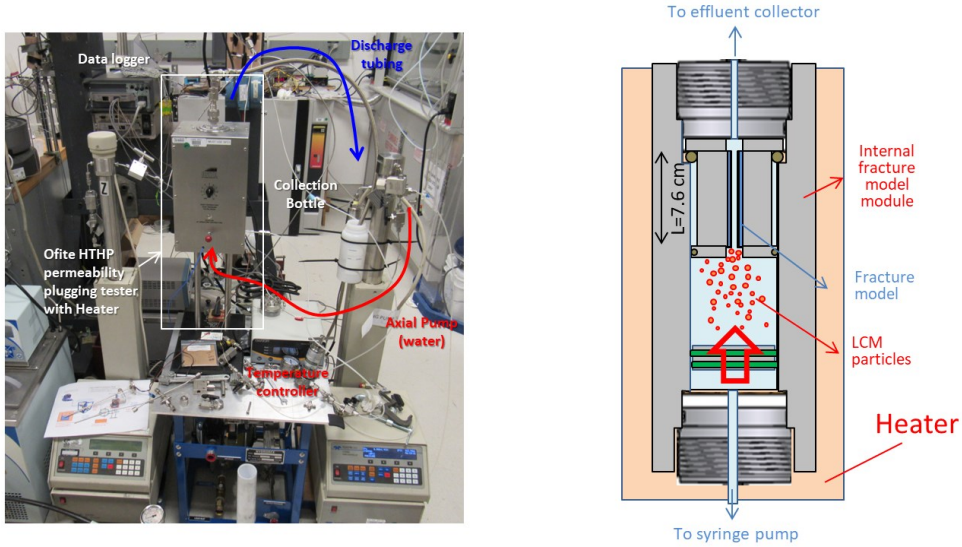

a. Test system using an Ofite permeability plugging tester b. An internal fracture module

Figure 3: Laboratory system used for fracture clogging experiments. Commercial equipment (Ofite permeability plugging tester) was used, with improvements to the temperature and flow/pressure controls. Additionally, the filter plate for testing clogging was replaced by a removable module which houses a fracture model.

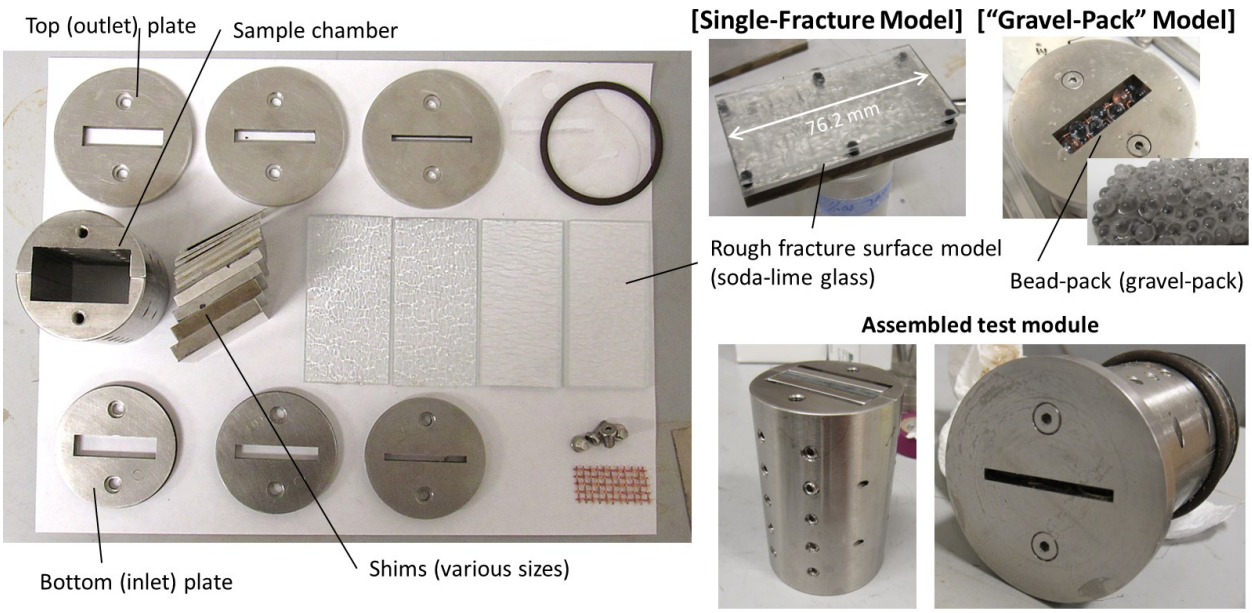

Figure 4: Internal fracture module made of stainless steel. A pair of plates with rough surfaces is used to represent a fracture with a finite depth, which is inserted in a rectangular cavity within the module. Alternately, the cavity can be filled with discrete particles (gravels, beads) to represent a rubble zone or a pack of coarse drill -cuttings and LCMs. The length of the module shown here is ~9 cm.

This module was designed so that a pair of thin plates (a 3.81 cm×7.62 cm×~3 mm model is shown in Figure 4) can be inserted to represent a nominally flat and parallel fracture. The fracture aperture can be changed by using Viton spacers and stainless steel shims on the back sides of the fracture plates. Tapered shims can be used to represent a fracture with varying (reducing) apertures. Additionally, instead of using a fracture model and shims, the cavity of the module can be filled with large solid particles such as gravels and beads to represent a fractured zone or a pack of large particles including drilling chips and carbonate chip LCMs.

Although natural rock samples can be used for the fracture model, in this study, we used transparent soda-lime glass plates with a manufactured surface texture (i.e., commercially available shower-window glass sheet). This allowed us to visualize the distribution of the LCM that penetrated into the fracture during the post-experiment examination of the samples, as well as to conduct quantitative mapping of the fracture aperture distribution via a UV-light-induced fluorescence intensity mapping of the fluid injected in the fracture (e.g., Nakagawa and Borglin, 2019).

The permeability (or conductivity) of a model fracture can be determined by testing the hydraulic conductivity of the fracture module independently by using a standard hydraulic permeability test such as falling-head permeability test. In our experiment, glass plates with a range of separation distance were used in the fracture module to determine equivalent hydraulic apertures of the rough model fractures.

2.2 Experimental Procedure

Because of circulation, the temperature of a borehole during drilling can be significantly lower than the reservoir, and can be below 100°C. Before an experiment, the test fluid containing LCMs was introduced in the pressure vessel, and the temperature was raised to 90°C within ~60 minutes. Once the temperature reached the target, the gas bubbles in the fluid were removed and the even distribution of LCM particles in the fluid was ensured by mechanical stirring. In the final step of the preparation, the gaps in the vessel and the fracture module were filled with hot water and then vessel was sealed, and the temperature was again raised to 90°C.

During an experiment, the injection pressure (representing the overpressure of the drilling fluid) was first raised to 10 psi (68 kPa), which approximately matched the pressure corresponding to the maximum friction of the test system. Subsequently, the injection pressure changed following a programmed constant pressure increase rate of 490 psi/min (56 kPa/s), with a flow rate limit of 100 mL/min (1.67 mL/s). Because of the limited volume of the LCM-fluid mixture stored in the vessel, the maximum volume of the injected fluid was limited to ~200 mL. If the target pressure (500 psi or 3.45 MPa) was reached, the pressure was maintained for 30 minutes, then reduced to ambient in 1 minute. Throughout the experiment, the temperature, fluid pressure, volume and the flow rate were monitored and recorded by a multichannel digital multimeter (Keithley DMM6500).

2.3 Experimental Results

2.3.1 Micro-C tests

First clogging experiments were conducted for coarse type micro-C (size ~0.8 mm), fine type micro-C (D50=~50µm), and their equal-weight mixture. As shown in Figure 5, for a "narrow" fracture with a hydraulic aperture (equivalent to flat parallel plates) of h_H=0.75 mm, both fine and coarse micro-Cs failed to clog the fracture and stop the fluid loss, resulting in depletion of the injected fluid. Examination of the sample showed that fine micro-C simply flowed through the fracture. The coarse micro-C did form a filter cake at

the fracture inlet, but the mud filtered through the pore space. In contrast, the mixed micro-C both formed a filter cake and stopped the fluid loss very effectively. In Figure 5, the fluid loss history indicates that near-complete clogging occurred at a pressure as low as ~100 psi (0.69 MPa). However, for a wider-aperture fracture (h_H=1.71 mm), the mixed micro-C could not stop the fluid loss, because no filter cake could form. Note that the D50 was less than 0.5 times the fracture aperture.

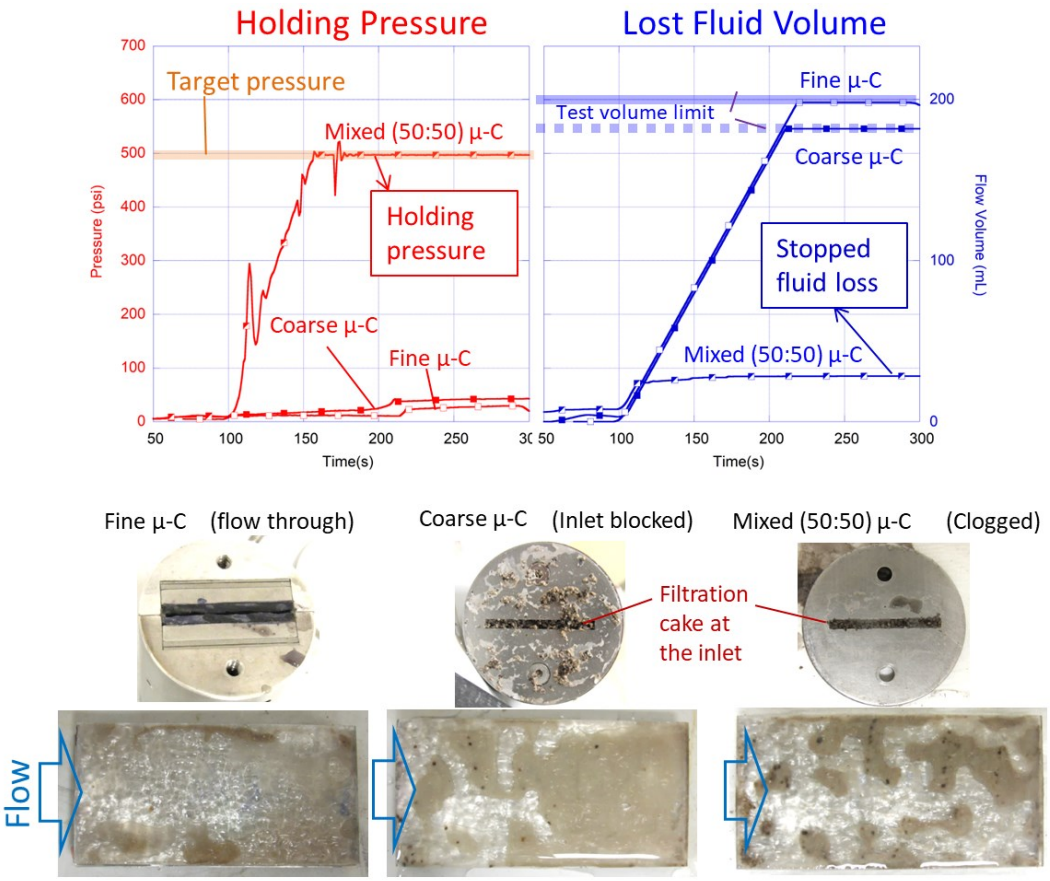

Figure 5: Micro-C clogging tests ("Narrow" fracture with h_H=0.75 mm). Fine micro-C just flowed through the fracture. Coarse micro-C formed a filtration cake by blocking the entrance, but did not slop the fluid loss. In contrast, combined use of both micro-Cs was highly effective in clogging the fracture with minimum loss.

2.3.2 Single-type LCM tests

Next, different types of LCMs with wider grain-size distributions were tested on a wide-aperture fracture (h_H=1.71 mm). In this case, both cotton-seed hulls and cedar fibers LCM behaved similar to the coarse micro-C on a narrow fracture, forming a filtration cake but not successfully stopping the fluid loss (Figure 6). In contrast, saw dust and WCA-type LCMs exhibited rapid oscillation of the injection pressure, which indicates that an unstable filtration cake formed, which can withstand some levels of differential fluid pressure and reduce the fluid loss. During the duration of the fluid loading, however, stable clogging was not achieved. The images of the fractures after the experiment confirm that the both filtration cake formation and penetration of the LCM into the fracture occurred.

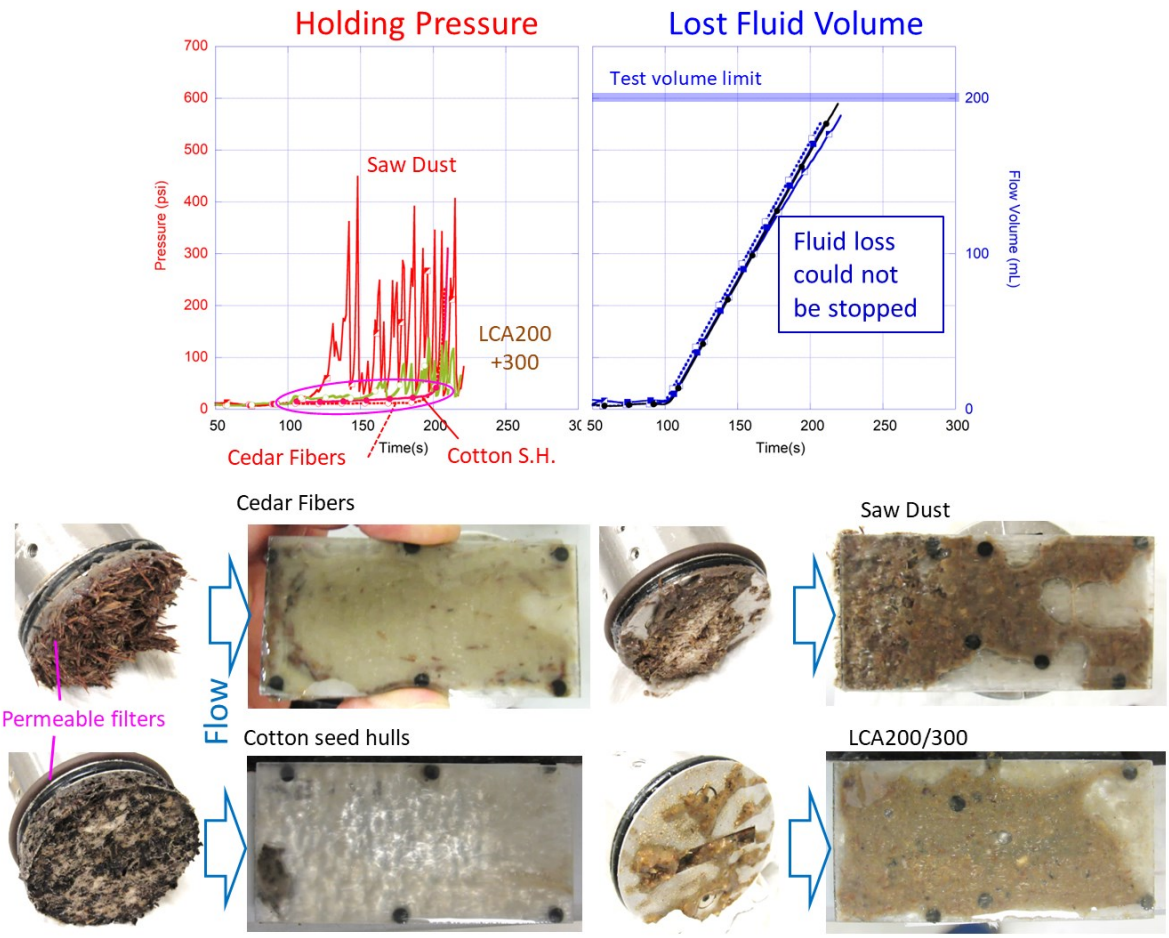

Figure 6: Single-type LCM tests ("Wide" fracture with h_H=1.71 mm). Cedar fibers and cotton seed hulls formed a thick filtration cake, but could not stop the fluid loss. In contrast, saw dust and WCA resulted in intermittent clogging, which was indicated by rapid pressure oscillations and the LCMs penetrated into the fracture. However, the target fluid pressure could not be reached.

2.3.3 Dual-type LCM tests

Mixing different types of LCMs helps broaden the particle size distribution, and also takes advantages of unique roles played by different types of LCMs. Based upon the performance of the single-type LCMs, we observed that both cotton seed hulls and cedar fibers are effective in forming a filter cake over a wide-aperture fracture (i.e., effective "bridging") while saw dust can clog the pore throats within the filter cake (i.e., effective "sealing"). Note that the WCA-type LCM is a blend of multiple types of LCMs with a range of particle sizes. Here, we used mixtures consist of cotton seed hulls and saw dust, cedar fibers and saw dust, and cedar fibers and fine micro-C powders, on a wide aperture fracture (h_H=1.71 mm).

The first two samples (mixture of cotton seed hulls and saw dust, and cedar fibers with saw dust) both successfully stopped the fluid loss, with the first type (cotton seed hulls + saw dust) being more effective and resulting in faster clogging and less fluid loss (Figure 7). In contrast, although a filter cake did form, the combination of cedar fiber and micro-C powder could not stop the loss, because the fine powder leaked through the pore space between the packed cedar fibers. The photographs of the fractures after the experiment show that, unlike the filter cakes that failed to stop the fluid loss, the cotton seed hull and cedar fiber filter cakes in these experiments show penetration of the filter cake into the fractures, possibly thanks to the increased differential pressure across the filter.

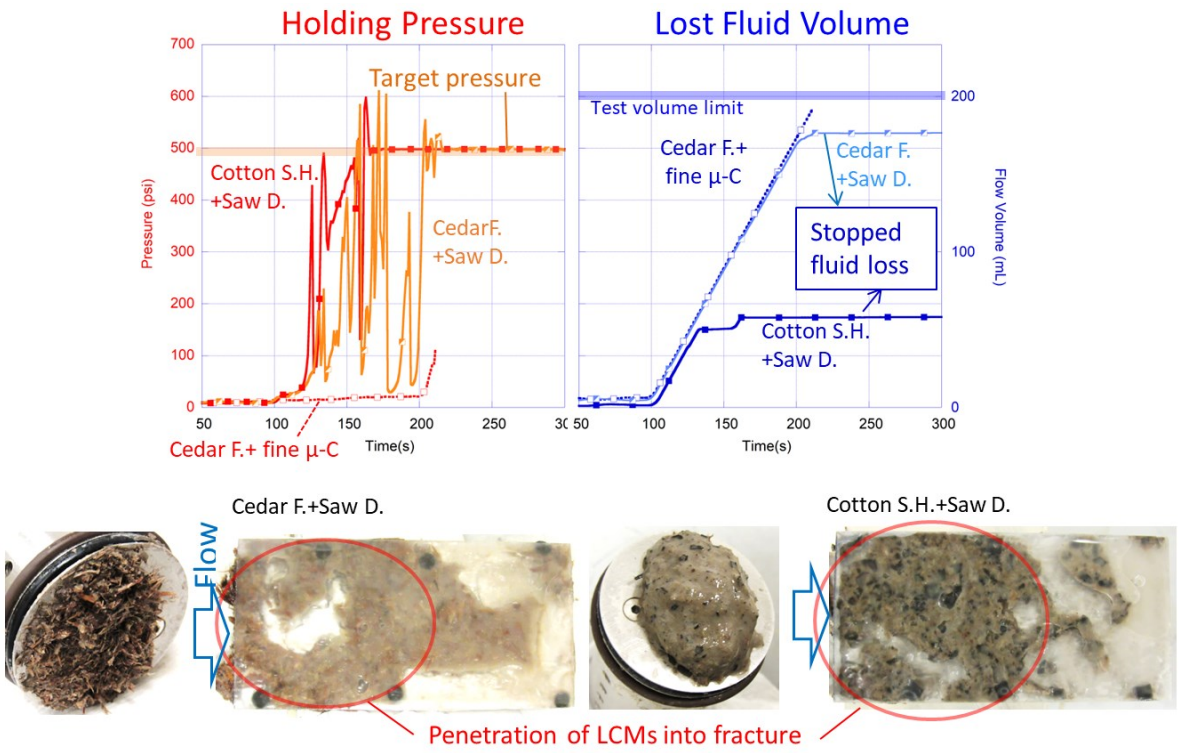

Figure 7: Dual-type LCM tests ("Wide" fracture with h_H=1.71 mm). By combining saw dust with cedar fiber and cotton seed hulls, the fracture was clogged effectively and the fluid loss was stopped. The increased fluid pressure also resulted in penetration of the filter cake deeper into the fracture. In contrast, a dual-LCM consisting of fine micro-C and cedar fibers could not stop fluid loss, because the fine micro-C powder flowed through the cedar fiber filtration cake.

3. LCM COMPACTION MODELING

We realize that the formation of a filter cake and subsequent clogging by LCMs is a complex process involving large deformation (strains) and porosity and permeability reduction of the porous media. For better understanding of this process and to gain insight into the relative efficiency of clogging by different types of LCMs, in this section, we examined their compaction behavior in detail.

3.1 Model Setup

First, we consider a one-dimensional consolidation model shown in Figure 8a. At the resting state, a porous medium (LCM) has an initial thickness H_0 and a permeability k_0. There is a fluid reservoir on its left, and a permeable, fixed (zero-displacement) boundary on the right. When a differential pressure P is applied between the fluid reservoir and the fixed boundary, the resulting flow (with a Darcy velocity V_f) induces varying fluid pressures p_f within the filter cake. Because the effective stress increases from the left boundary in contact with the reservoir to the right boundary pressed against a permeable wall, both strain and permeability changes increase monotonically. To make the modeling simple, we make following assumptions:

- The effective stress coefficient α=1, which is used to compute the effective compressive stress $Pc=P-\alpha p_f$
- The segment length (or volume) change is given by a nonlinear function $dh/dh_0=f(Pc)$
- The permeability change of the segment is given by a nonlinear function $k/k_0=g(Pc)$

Next, for modeling a filter cake forming at the entry to a straight fracture (with an infinite length) in Figure 8b, we make an additional assumption:

- The segment volume change is given by a nonlinear function $(\pi r dr)/(\pi r_0 dr_0)=f(Pc)$

Note that this assumption may be rather unrealistic because it ignores the effect of hoop stress, but we will accept it as an approximation based upon the 1D model.

For both cases, the model is spatially discretized in the length (h) or radial (r) direction, and Darcy's law is applied locally to compute the effective stress distribution and the resulting deformation and permeability. These are in turn used to compute the changes in the flow rate and pressure distribution across the filter, which are again used to compute the local pressure gradient (drop) and the effective stress. Through this iterative process, for a given input differential pressure P, the internal distribution of the pressure, permeability, and deformation, and the overall flow rate across the LCM filtration cake are determined (Figure 9).

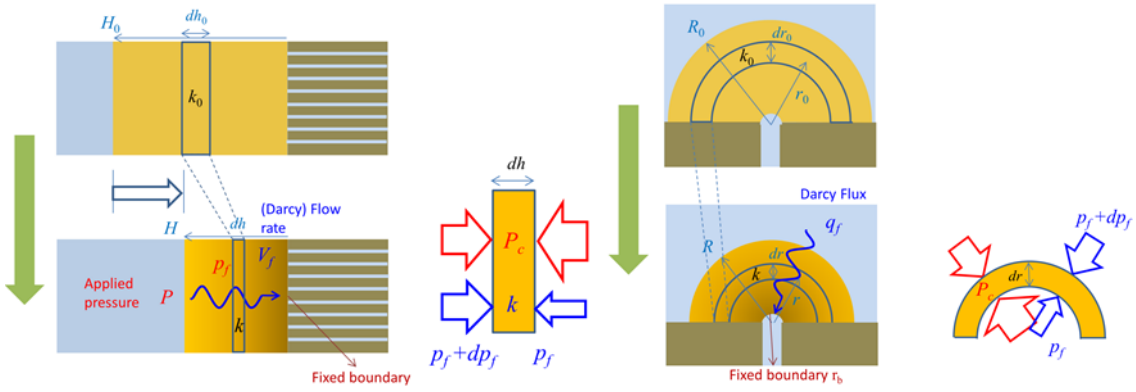

a. b.

Figure 8: Consolidation (compaction) models used for LCM plug formation problems. These models examine the compaction and formation of a filtration cake by the fluid pressure difference between a borehole and the reservoir rock. The flow-induced gradient in the effective stress causes spatially varying permeability and compaction.

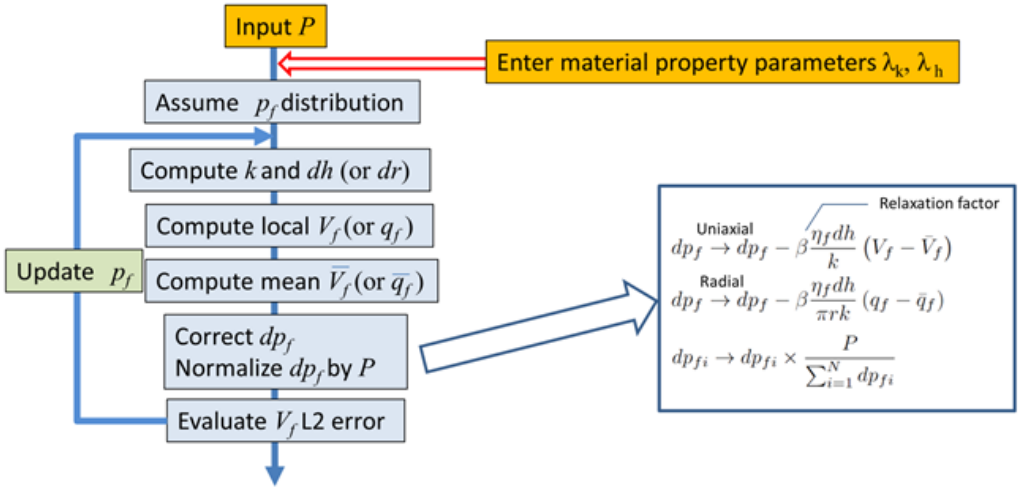

Figure 9: Solution steps for computing internal pressure distribution and overall flow rate. For an applied external pressure, a spatially varying pressure distribution which locally satisfies the Darcy's law is determined iteratively.

3.2 Modeling Results

In the following, we will provide some examples of predicted, applied overall pressure (P) – flow rate (V_f) relationships for the radial LCM filter cake model in Figure 8b. Although we do not show the results for the 1D model here, they are qualitatively very similar to the radial model. In these simulations, we assume a fracture width =1 mm, filter cake thickness (radius) 5mm, initial permeability 100 D, and fluid viscosity 10 cP. For the nonlinear deformation and permeability function $f(P_c)$ and $g(P_c)$, we assume simple exponential functions

$$f(P_c) = \exp(-\lambda_h P_c), \quad (1)$$

$$g(P_c) = \exp(-\lambda_k P_c). \quad (2)$$

In Eqs. (1) and (2), P_c is the effective stress, and λ_k and λ_h are the exponential decay rates of the permeability and the bulk sample volume, respectively. Additionally, for easy comparison, we assume the same rate of change for deformation $1/\lambda_h$=100 psi (0.69 MPa), and vary the relative magnitude of λ_k.

Case I: Similar deformation and permeability change rates

We assume $\lambda_k = \lambda_h$ (Figure 10a). In this case, the rate of increase of overall filtration flow rate somewhat decreases with increasing applied pressure. Because of the both effective-stress-dependent changes in the permeability and the geometry of the converging flow, the pressure profile becomes increasingly nonlinear with increasing pressure at the boundary.

Case II: Permeability change faster than deformation change

For this case, we assume $\lambda_k = 10\ \lambda_h$ (Figure 10b). Quite interestingly, the flow-rate increase reaches a plateau, then collapses to zero at high applied pressures. Note that, because the strong pressure gradient and the resulting increase in the effective stress concentrates only

near the outlet (near location=0), the pressure profile is nearly flat, and the overall deformation of the filter cake shown by the red closed circles is minimal.

Case III: Deformation change faster than permeability change

In the third case, we assume $\lambda_k = 0.1\ \lambda_h$ (Figure 10c). In this case, the rate of increase of the filtration flow rate increases with the applied pressure. This may appear aphysical, although can happen because of the rapid reduction in the flow path length.

To clearly show how the changes in the parameters affect the filtration flow rate vs. applied pressure relationship, for the same test parameters, the resulting curves are shown for a range of λ_k/λ_h values in Figure 11.

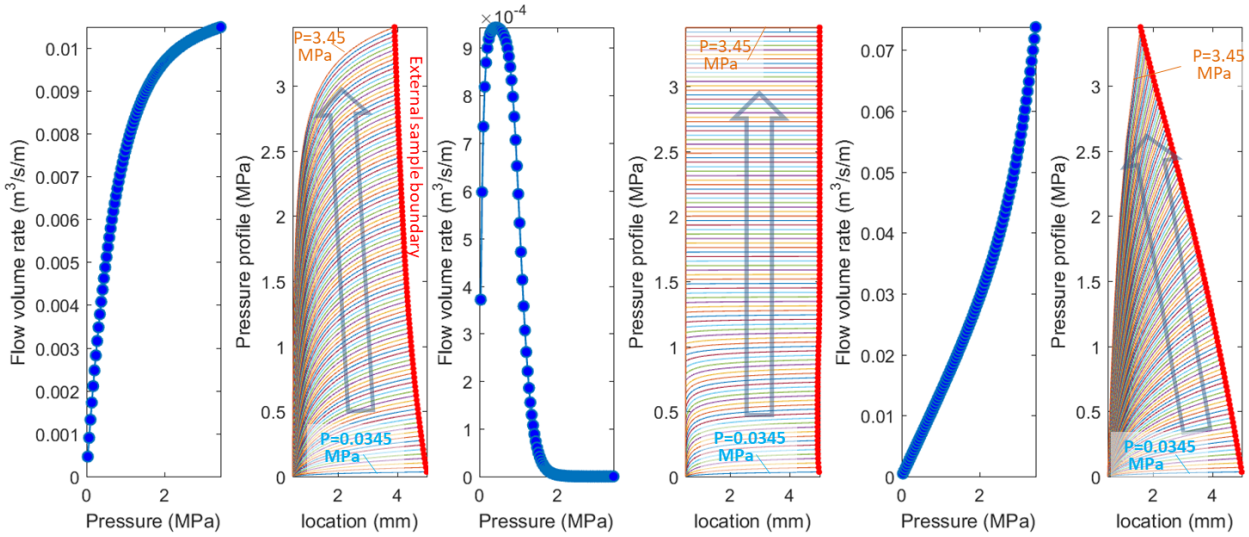

a. Case I: $\lambda_k = \lambda_h$. b. Case II: $\lambda_k = 10\,\lambda_h$. c. Case III: $\lambda_k = 0.1\,\lambda_h$.

Figure 10: Overall filtration flow rate and pressure profile behavior against increased differential pressure, for different exponential decay rates for the LCM volume and the permeability. Multiple lines for the pressure profiles correspond to each pressure value in the flow volume rate to pressure plots. The locations of the external boundary of the filtration cake are also shown in closed red circles. When the reduction of the permeability is much faster than compaction of the sample (b), the overall permeability of the filtration case "collapses", exhibiting a very rapid drop in the flow rate with increasing externally applied fluid pressure.

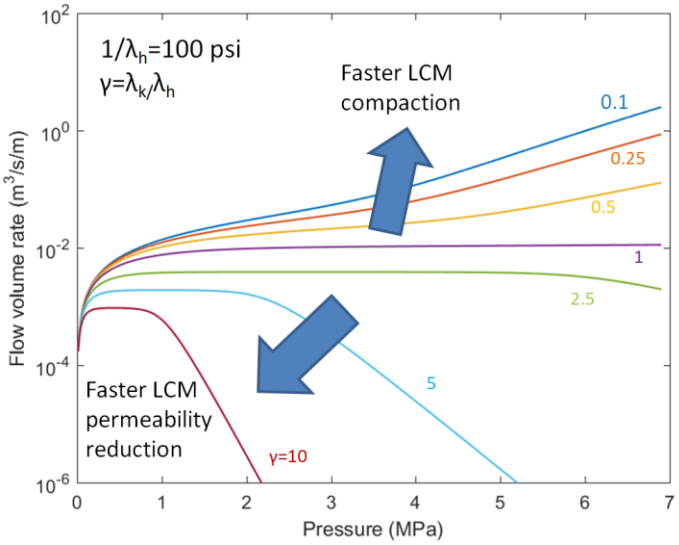

Figure 11: Comparison of the filtration volume rate vs. applied pressure for a range of exponent ratios λ_k/λ_h. When the permeability reduction is less sensitive to pressure changed compared to LCM compaction, increase in the pressure results in increase in the flow rate. For $\lambda_k \sim \lambda_h$, the flow rate reaches a plateau (i.e., becomes independent of the pressure). For very fast permeability reductions compared to sample compaction, collapsing permeability (increase in applied pressure results in reduction of flow rate) emerges.

4. DISCUSSION AND CONCLUSION

Laboratory fracture clogging experiments in Section 2 demonstrated the importance of LCM grain size and its distribution. Generally, coarse LCM particles provide a filtration cake via bridging effect, then fine LCM particles stops the flow via a sealing effect. For fractures with very large apertures, drill chips and even coarser LCMs (such as carbonate chips) can provide a larger-scale bridging effect. Successful clogging of the sealed filtration cake, which can stop fluid loss efficiently, also depends on its mechanical stability. Unstable filtration cake can lead to cycling formation of the filter and its collapse, resulting in incomplete fracture clogging, which manifests itself as pulsating fluid pressure and flow rate. The experiment indicated cyclic clogging by filtration cake formation and de-clogging due to its collapse for relatively large fracture apertures compared to the nominal LCM size.

Mixing of different types of LCMs led to improved performance, achieving both collapse-resistant bridging and sealing of the filtration cake. We found that combinations of cotton seed hulls or cedar fibers as the bridging material, and saw dust as the sealing material, to be particularly effective, although the grain sizes of the tested materials were not controlled in our experiment.

Finally, the preliminary numerical modeling indicates one possible mechanism which makes a particular LCM (or a combination of LCMs) highly effective. Currently, the flow and deformation behavior of the LCM samples used in this study is being characterized, in order to compare the model predictions against the actual performance of the LCMs in the fracture clogging tests.

ACKNOWLEDGMENTS

This work is supported by the U.S. Department of Energy, Office of Energy Efficiency and Renewable Energy (EERE), Office of Technology Development, Geothermal Technologies Office, under Award Number DE-AC02–05CH11231 with LBNL and contract DE-NA0003525 with SNL. Sandia National Laboratories is a multi-mission laboratory managed and operated by National Technology & Engineering Solutions of Sandia, LLC, a wholly owned subsidiary of Honeywell International Inc., for the U.S. Department of Energy's National Nuclear Security Administration. This paper describes objective technical results and analysis. Any subjective views or opinions that might be expressed in the paper do not necessarily represent the views of the U.S. Department of Energy or the United States Government. The authors would like to thank Drs. John Tuttle and Ron Tate (Sinclair Well Products) and Dr. Lyndon Chandarjit (North Star Energy Products) for providing the commercial LCMs used in the research. We would also like to thank Prof. Saeed Salehi (University of Oklahoma) and his research group, and Drs. Mike Otto and Stephen Bruce (Baker Hughes) for valuable advice and suggestions regarding laboratory testing of LCMs. SAND2023-12421C.

REFERENCES

Alsaba, M., Al Dushaishi, M.F., Nygaard, R., Nes, O-M., and Saasen, A.: Updated criterion to select particle size distribution of lost circulation materials for an effective fracture sealing, Journal of Petroleum Science and Engineering 149, (2017), 641–648.

Berne, B. J., and Pecora, R.: Dynamic light scattering: with applications to chemistry, biology, and physics, Courier Corporation, (2000), ISBN 0-486-41155-9

Kibikas, W., Chang, C., Bauer, S.J., Nakagawa, S., Dobson, P., Kneafsey, T., and Samuel, A.: Thermal degradation and mixture properties of materials used for lost circulation management, Proceedings, 48th Workshop on Geothermal Reservoir Engineering, Stanford University, Stanford, California, (2023).

Nakagawa, S., and Borglin, S.E.: Laboratory In-Situ Visualization of long-term fracture closure and proppant embedment in brittle and ductile shale samples, In 53rd US Rock Mechanics/Geomechanics Symposium, New York, New York, ARMA 19-1996, (2019).

Lowry, T., Winn, C., Dobson, P., Samuel, A., Kneafsey, T., Bauer, S., and Ulrich, C.: Examining the monetary and time costs of lost circulation, Proceedings, 47th Workshop on Geothermal Reservoir Engineering, Stanford University, Stanford, California, (2022).

Vivas, C., and Salehi, S.: Screening of Lost Circulation Materials for Geothermal Applications: Experimental Study at High Temperature. Journal of Energy Resources Technology, 144(3), (2022).

Winn, C., Dobson, P., Ulrich, C., Kneafsey, T., Lowry, T. S., Akerley, J., Delwiche, B., Samuel, A., and Bauer, S.: Context and mitigation of lost circulation during geothermal drilling in diverse geologic settings, Geothermics, 108, (2023), 102630. doi:https://doi.org/10.1016/j.geothermics.2022.102630